Fluorine-Doped Tin Oxide/Alumina as Long-Term Robust Conducting Support for Earth-Abundant Water Oxidation Electrocatalysts

Felipe A. Garcés-Pineda, Jesús González-Cobos, Mabel Torrens, and José R. Galán-Mascarós

In this work we apply a novel and simple methodology to develop a composite that consists of anodic aluminum oxide (AAO) covered by a fluorine-doped tin oxide (FTO) film. The composite presents suitable morphological and electrical properties to be used as support for water electrooxidation catalysts based on non-noble metals. AAO substrates were decorated with FTO via spray pyrolysis, followed by deposition of catalyst nanoparticles consisting of a cobalt-analogue of Prussian Blue that promotes the oxygen evolution reaction. The electrodes were characterized by X-ray Diffraction, Environmental Scanning Electron Microscopy and resistivity measurements. A promising electrocatalytic activity of the optimized AAO/FTO/PB electrode was observed at neutral pH and ambient conditions. The obtained results open a feasible strategy in the search for competitive water oxidation electrodes based on the combination of earth-abundant metal catalysts on FTO-covered anodized alumina supports.

1. Introduction

Porous anodic aluminum oxide (AAO) has been extensively studied for the last years in different fields in nanoscience and nanotechnology.[1–2] AAO is a honeycomb-like porous material formed by electrochemical anodization of aluminum in an acid electrolyte. As a result, an ordered nanoporous structure with very high surface area is obtained. Moreover, this material is mechanically, chemically and thermally stable. AAO hardness, corrosion resistance and erosion resistance have shown to be improved after the aluminum anodization process.[3] For instance, AAO is attractive as template or host material for the growth of ordered nanotube or nanowire arrays for electrochemical applications like energy storage and conversion.[4] As a few examples, AAO templates have been used to fabricate a nanostructured CdS-CdTe solar cell[5] or a photoanode for water splitting based on Fe_2TiO_5 nanotubes.[6] In these cases the AAO support is removed after the deposition of the guest material leading to free-standing nanoporous structures. The AAO removal is typically performed by immersing the composite material into a concentrated NaOH or H_3PO_4 solution. There are several examples of nanoporous electrodes obtained in this way which have been tested for different electrocatalytic reactions such as electroreduction of chloroform,[7] hydrogen evolution reaction,[8] electrooxidation of hydrazine,[9] urea,[10] methanol[11–12] or ethanol.[13] However, since AAO is electrically insulator, it is not common the use of this material as permanent support for electrocatalysts and, in general, for applications where high electrical conductivity is required. In these cases, AAO needs to be appropriately assembled with a conductive component. For instance, Altuntas and Buyukserin obtained an AAO modified with carbon to develop a biomaterial nerve tissue,[14] and Wierzbicka and Sulka used an Au-covered AAO as sensitive electrode for electrochemical determination of epinephrine.[15]

In the present study our interest is focused on the application of AAO in water electrolysis, since one of the main bottlenecks in this field is the search for stable electrodes able to survive to challenging redox and pH conditions.[16–18] Noble metal electrodes are traditionally used for water oxidation, specially at low pH.[19–20] Ni-based electrodes are preferred at high alkaline pH[8,21] but they rapidly get oxidized when the pH is lowered. Carbon electrodes are pH-stable but unstable during oxygen evolution catalysis.[22] In this sense, AAO can be an alternative. This material has been recently used as support of Ir[23–24] and Pt[24] catalysts for water oxidation in acidic media, demonstrating the stability of AAO-supported catalysts under electrooxidation conditions. Other current bottleneck in the development of water electrolysis technology is precisely the substitution of this kind of noble, expensive catalysts. Increasing efforts are being made towards the implementation of Earth-abundant transition-metal oxides.[18,25–26] In this context, a cobalt-analogue of Prussian Blue (PB), cobalt hexacyanoferrate (CoHCF), has been reported as a good candidate as water oxidation catalyst showing an efficient and robust activity.[27–32] Herein we aim to use anodic aluminum oxide as support for Prussian Blue nanoparticles. However, AAO/PB electrodes could

]

Dr. F. A. Garcés-Pineda, Dr. J. González-Cobos, Dr. M. Torrens, Prof. J. R. Galán-Mascarós
Institute of Chemical Research of Catalonia (ICIQ)
The Barcelona Institute of Science and Technology (BIST)
Av. Països Catalans, 16, Tarragona, 43007 Spain
E-mail: fgarces@iciq.es
jcobos@iciq.es
Prof. J. R. Galán-Mascarós
ICREA
Passeig Lluis Companys, 23, Barcelona, 08010 Spain

Supporting information for this article is available on the WWW under https://doi.org/10.1002/celc.201900218

not be directly used as anodes for water splitting given the electrically insulating character of this hypothetical composite. Our strategy in the present work consists of a controlled deposition of a conductive material over the AAO surface before the PB addition. SnO_2 is one of the most studied members in the family of transparent conductive oxides (TCO) and, particularly, F-doped tin oxide (FTO).[6,33–36] Besides its transparency in the visible region of the electromagnetic spectrum and low electrical resistance, it can be easily deposited on different surfaces by spray pyrolysis.[35–36] We propose for the first time in literature the use of FTO-covered AAO as water oxidation catalyst support. In this way, it is expected that FTO provides a suitable electrical conductivity on the surface and that AAO induces an increase in the rugosity and number of defects of the FTO layer. AAO/FTO composites with different FTO layer thicknesses have been characterized in terms of surface morphology and electrical properties, and CoHCF nanoparticles supported on the optimum AAO/FTO substrate have exhibited a promising performance for water splitting at neutral pH. The results shown below indicate that AAO/FTO is a viable, efficient and long-term robust electrode to support non-noble water oxidation catalysts.

2. Results and Discussion

Porous alumina substrates were modified by depositing fluorine-doped tin oxide (FTO) layers by spray pyrolysis. SnO_2:F coverage was controlled by varying the deposition time. Figure 1 shows the scanning electron microscopy (ESEM) images for AAO/FTO samples after 10 and 120 min deposition. One can observe that AAO surface is covered by FTO nanograins and both the number and the size of these grains show to be increased along the deposition time, finally obtaining a fairly uniform layer composed of FTO grains with diameters of the order of μm. A similar FTO grain dependence on deposition time was recently shown by other authors on glass substrate.[37]

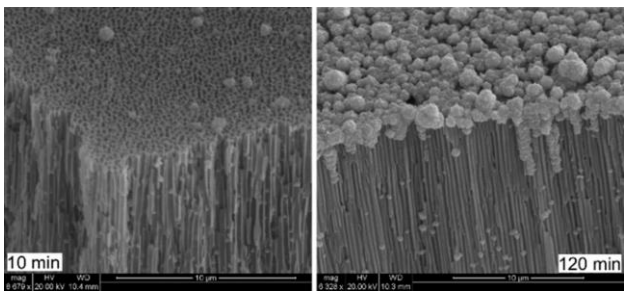

Figure 1. ESEM images from two different layers of AAO/FTO template. On the left, an AAO substrate with a FTO layer obtained after 10 minutes of deposition time. On the right, an image with the FTO deposited for 120 minutes.

The AAO/FTO pore size is also reduced along FTO deposition, as it can be observed in Figure 2. The bare AAO template used herein presents an average pore size of c.a. 220 nm and

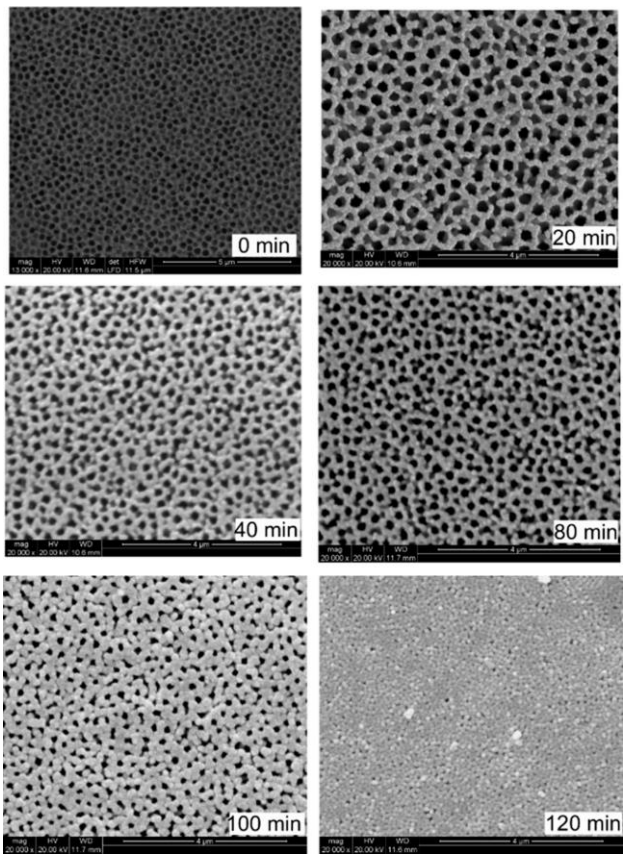

Figure 2. ESEM images in top view from samples obtained after different deposition times of FTO onto AAO templates.

finally, after 120 min, the AAO outermost surface seems to be almost fully covered by FTO without apparent open pores (maximum pore size of c.a. 50 nm). This effect may be linked to the grain nucleation. For longer times (i. e. thicker FTO layers) the adatoms coalescence increases and this directly affects the crystal growth. In the AAO/FTO sample prepared for 120 minutes it can also be appreciated a high roughness on the membrane surface.

A partial penetration of FTO into the alumina pores is confirmed from the cross-section image shown in Figure 3, where several EDX spectra were taken at different depths in the AAO. Although FTO signal decreased along the pore depth, it can be observed that FTO penetration takes place at least 20 μm in depth. Despite this, on the basis of these micrographs one can anticipate that the FTO coverage is mostly produced on the AAO outermost surface in contrast, for example, to a previous study where a nanotubular electrode was obtained by introducing FTO into the channels of an AAO substrate.[38] It was possible in this case due to a larger initial pore diameter of AAO, c.a. 900 nm (vs. c.a. 220 nm in the present work). Despite the high specific surface area of the bare AAO substrate employed herein, the pore diameter is not wide enough to allow the full covering in depth by FTO during the spray pyrolysis deposition. Thus the AAO/FTO/PB electrodes tested below probably present lower active surface area than other

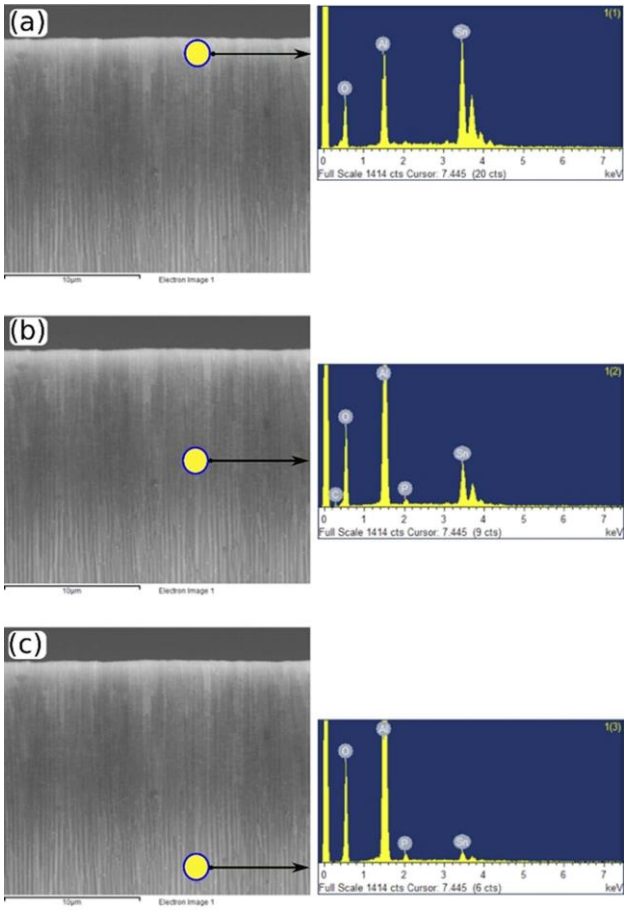

Figure 3. ESEM image in cross section of the AAO/FTO layer deposited for 120 min along with EDX spectra obtained at a) c.a. 1 μm, b) c.a. 10 μm and c) c.a. 20 μm in depth.

ICSD database) which are shown as vertical dotted lines in Figure 4a. This indicates the presence of the tetragonal phase of SnO_2 with the characteristic crystalline directions such as [1 0 1], [2 0 0] and [2 1 1]. The Full Width at Half Maximum (FHWM) parameter decreases for longer deposition times which indicates an increase of the FTO crystallite size. This is confirmed in Figure 4b, where the values calculated from the Scherrer equation are shown. The crystallite size increases from c.a. 8 to c.a. 19 nm along the deposition time.

Electrical characterization of the AAO/FTO samples was also performed by means of a method based on I–V characteristics obtained in a planar configuration (see inset of Figure 5) which

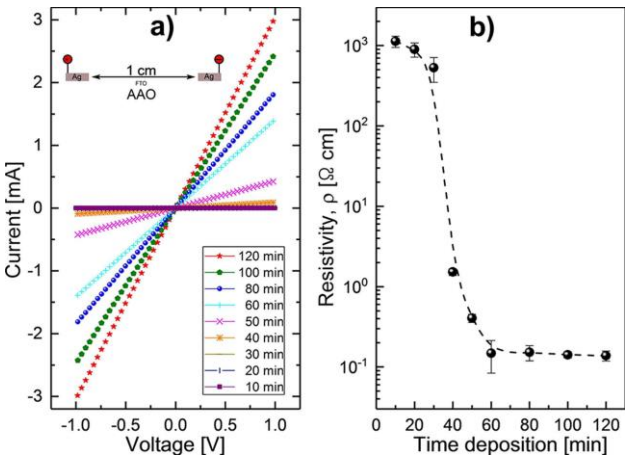

Figure 5. a) I–V characteristic for two AAO/FTO layers after different deposition times. b) Electrode resistivity decrease with the FTO layer thickness increase. The inset of this figure shows the setup configuration employed for these measurements.

electrodes that could be prepared by using AAO supports with larger initial pore diameter.

Structural analysis of the samples by X-ray diffraction (XRD) was also carried out. The XRD patterns (Figure 4a) reveal the polycrystalline nature of the FTO films with no preferential orientation. The diffraction peaks are coincident with those of the Cassiterite phase (reference 1-072-1147, reported in the

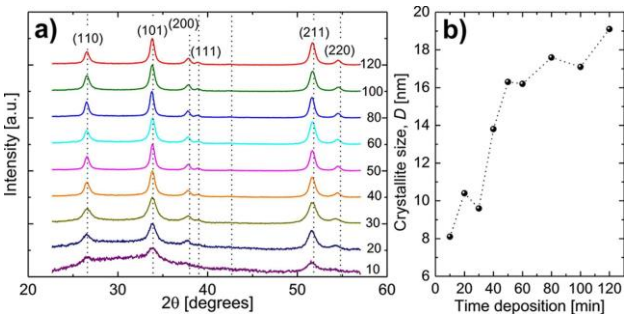

Figure 4. a) X-ray diffraction patterns for different deposition times of FTO onto AAO membranes. The dotted lines correspond to the reference 1-072-1147 reported in the ICSD database. b) Crystallite size dependence on deposition time.

has also been applied in other works.[14] In Figure 5a it can be observed the I–V curve for the different AAO/FTO composites, from whose slope the sheet resistance can be obtained. First this value decreased sharply from 3.24×10^7 Ω/sq (on the FTO layer deposited for 10 min) to 708 Ω/sq (on the one deposited for 60 min) and, from then, it continued slightly decreasing up to reach 330 Ω/sq (on the FTO layer deposited for 120 min). This decrease in the electrical resistance can be attributed to the influence of the deposition time in the achievement of larger FTO grains and a more intimate contact between grains which may improve the carrier transport. The higher the grain size and the higher the grain connectivity, the lower the sheet resistance, as it has also been observed by other authors on FTO layers deposited on glass substrates.[35,37,39] Figure 5b shows the evolution of the resistivity along the FTO deposition time. This parameter was estimated from the sheet resistance values and the corresponding thickness of the FTO layers. The thickness increased during the deposition procedure up to reach 2.1 μm onto each AAO side after 120 min and the growth rate of the FTO layer was estimated at c.a. 35 nm min^{-1}. One can observe a sharp decrease of resistivity of four orders of magnitude, to 0.149 Ω cm, for the first 60 min of FTO deposition. The decrease of the resistivity with the increase of the FTO

thickness has also been reported in other works.[37,40] However, in contrast to the sheet resistance trend, the resistivity remained fairly constant from this moment and it was finally measured at 0.138 Ω cm after 120 min.

CoHCF nanoparticles were deposited onto the different AAO/FTO supports following the same dip-coating procedure in each case, as described in the experimental section. Figure 6

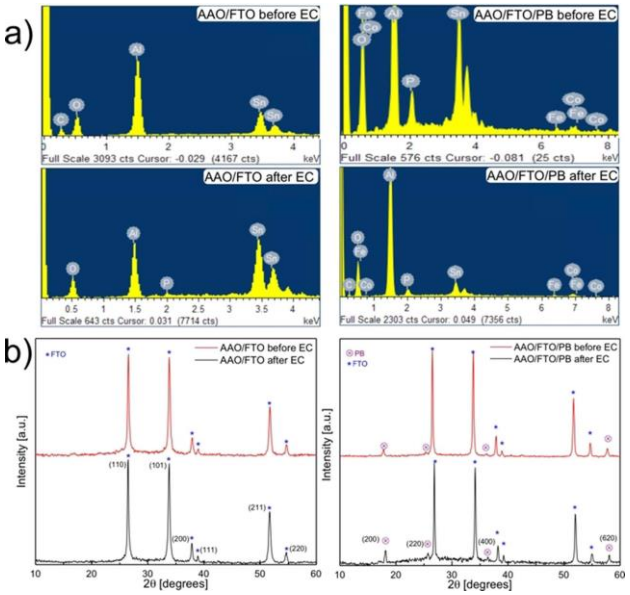

Figure 6. (a) EDX spectra and (b) XRD diffractograms from AAO/FTO/CoHCF electrode (120 min, 330 Ω/sq) both before and after the electrocatalytic tests.

shows the XRD and EDX spectra of the AAO/FTO/PB electrode (with FTO layer deposited for 120 min) and the AAO/FTO (blank) electrode, both in the fresh state and after being used for the electrocatalytic tests. In the EDX spectra (Figure 6a) the incorporation of Fe and Co atoms clearly appears in the PB-decorated AAO/FTO electrode. In the XRD diffractograms of the AAO/FTO sample (Figure 6b, left) the same six FTO diffraction peaks that were observed in Figure 4a are identified. In the case of the AAO/FTO/PB sample (Figure 6b, right), four new diffraction peaks are identified at $2\theta = 17.9°$, 25.4°, 36.3° and 58°, which can be attributed to Prussian blue and are characteristic of a face centered cubic structure.[41] Similar EDX and XRD patterns related to FTO and Prussian blue are found before and after the electrocatalytic measurements. This denotes that no significant catalyst leaching or change in phase took place, which confirms the stability of both the active electrode and the blank under the studied electrochemical conditions. Moreover, PB crystallite sizes of 15.7 nm and 14.5 nm are calculated from the diffractograms of the AAO/FTO/PB electrode before and after the electrocatalytic tests, respectively. This size is lower than that previously reported for other PB-based electrodes prepared by different deposition methods, i.e. drop-casting,[32] spray deposition,[31] electrodeposition[29] or a dip-coating procedure similar to the one employed herein.[30] In the present case the most influential feature seems to be the surface rugosity and high number of defects generated onto the AAO/FTO substrate which may lead to a large nano-structuring that allows the formation of such small PB crystallites. ESEM images were also obtained both before and after the electrocatalytic tests (see Figure S1 in Supplementary Information) and no apparent changes in electrode morphology can be appreciated.

Figure 7 shows the linear sweep voltammetry (LSV) performed in 50 mM potassium phosphate (KPi) electrolyte at

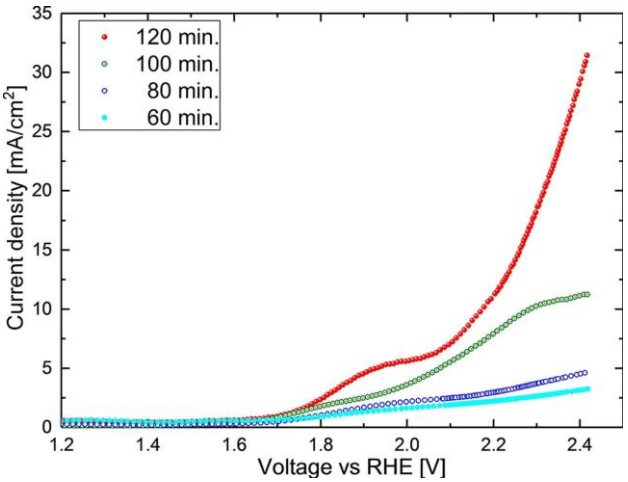

Figure 7. Linear sweep voltammetry for AAO/FTO/CoHCF electrodes with different FTO deposition times in 50 mM KPi electrolyte at pH 7.0.

pH 7.0 with the four AAO/FTO/PB electrodes with the FTO layers that showed lower resistivity values in Figure 5, i.e. those deposited for 60, 80, 100 and 120 min, in order to compare their electrocatalytic activity. The composite materials with FTO layers deposited for 60 and 80 min show negligible activity. The electrode with 100 min of FTO deposition shows a significant current density at the higher potentials, but the oxygen evolution curve is not well defined yet. The most active electrode is, by far, the one containing the FTO layer deposited for longest time, which reaches c.a. 32 mA cm^{-2} at 2.4 V vs. RHE. Taking into account that Prussian Blue catalyst was deposited for the same dip-coating time and that the obtained resistivity was the same in all these cases, one of the main reasons for the increase of the electrocatalytic activity with the FTO deposition time could be the surface roughness enhancement. The roughness has been typically found to increase with the thickness in studies on FTO films deposition by different methods[37,40, 42–43] and this feature can lead to an increase of the number of active Prussian Blue nanoparticles. Moreover, as the FTO deposition time is shorter, it is also plausible that these nanoparticles were deposited to a greater extent into the pores of the AAO/FTO composite. Although the specific surface area of the AAO support and the blocking extent of the pores by FTO were not quantified, the pore diameter left after FTO spray pyrolysis clearly decreases along deposition time, as observed in Figure 2. Hence, the electrodes with FTO layers deposited for less than

120 min likely lose most of the electrocatalytic activity from the CoHCF nanoparticles placed inside the AAO pores due to strong mass transfer limitations. In order to avoid mass transfer limitations in these cases different AAO substrates should be employed with higher initial pore diameter than that used in the present work (c.a. 200 nm).

Focusing on the case of the AAO/FTO/PB electrode with the FTO layer deposited for 120 min, one can clearly observe the typical exponential behavior due to water oxidation process after 2 V vs. RHE. Before this potential, a pre-oxidation peak is present at around 1.9 V vs. RHE. A similar peak is typically observed during LSV performed in other studies on water electrolysis with PB catalysts[28–29,32] and it can be attributed to an electron transfer process due to the $Co^{II}Fe^{II}$-$Co^{III}Fe^{II}$ couple. As it can be observed in Figure 8, the current density values

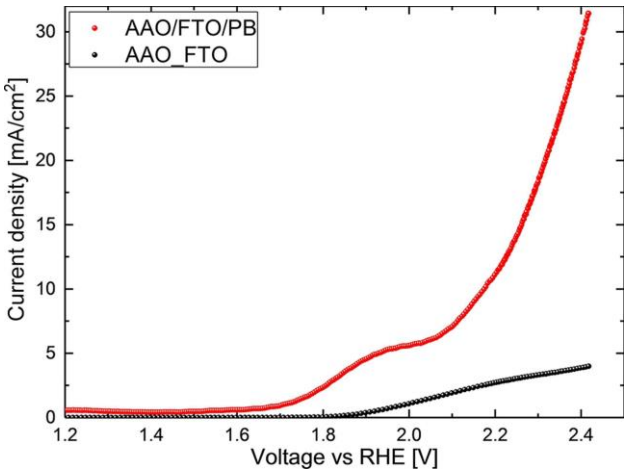

Figure 8. Linear sweep voltammetry for AAO/FTO/CoHCF electrode (120 min, 330 Ω/sq) in 50 mM KPi electrolyte at pH 7.0 (red line). Black line represents the blank substrate, AAO/FTO (i.e. without CoHCF).

obtained with the AAO/FTO/CoHCF electrode show to be much higher than those obtained with the AAO/FTO blank electrode, specially at higher potentials. This denotes that the electrocatalytic activity fairly proceeds from the PB nanoparticles.

In the Tafel plot (Figure 9) it can be observed a linear relationship between log j and the overpotential (η) in an η range of 0.3-0.5 V and 0.5-0.75 V for the AAO/FTO/PB and the AAO/FTO electrodes, respectively. In these regions the Tafel slope decreases from 99 mV/dec (blank electrode) down to 82 mV/dec for the PB-decorated substrate, which proves the catalytic process. In this kind of Prussian Blue-analogues the water oxidation catalytic activity is typically assigned to the Co centers while the function of the Fe centers is rather structural and electronic (enhancing stability and electron conduction).[28,32] It was previously demonstrated the competitiveness of PB-based electrodes in kinetic terms with respect to CoOx catalysts[29] and, very interestingly, the Tafel slope obtained with the AAO/FTO/PB electrode is even lower than the values previously shown at pH 7 by Aksoy et al.,[27] Alsaç et al.[28] and Pintado et al.[29] with other PB-based electrodes

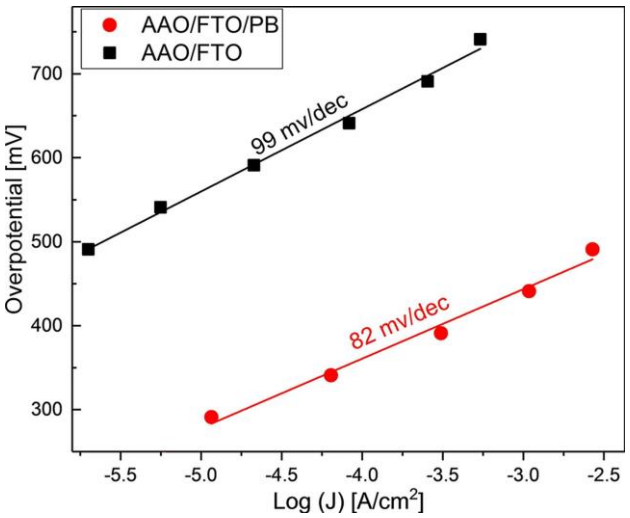

Figure 9. Tafel plot of the steady-state current density of the AAO/FTO/CoHCF and AAO/FTO electrodes in 50 mM KPi electrolyte at pH 7.0. The linear region shows the different Tafel slope for both electrodes.

prepared on flat substrates. The obtained electrocatalytic activity may be favored by the small PB crystallite size mentioned above but, specially, by the particular surface morphology of the AAO/FTO support. The use of this kind of porous support and the resultant roughness of the FTO conductive layer likely favor the presence of a higher amount of catalytic active sites leading to an improved electrocatalytic activity.

In order to check the long-term stability of the AAO/FTO/PB catalyst, a chronoamperometry (CA) was carried out for 100 hours under the same experimental conditions in the oxygen evolution voltage region, at 2.2 V vs. RHE (Figure 10). With both the AAO/FTO/PB and the blank electrode a sharp decrease of the current density is observed at the beginning of the CA, which is mainly due to the fast decay of capacitive current. The AAO/FTO sample showed a negligible activity

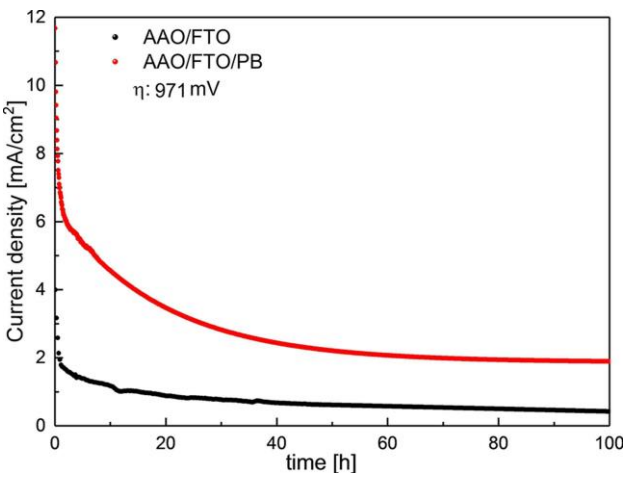

Figure 10. Bulk electrolysis of the AAO/FTO/CoHCF electrode at 2.2 V vs. RHE in 50 mM KPi electrolyte at pH 7.0, along with the blank measurement.

under steady-state conditions. In the case of the AAO/FTO/PB electrode, a slow decrease of current density is observed. One cannot totally discard some instability of the outermost FTO crystallites since the blank data shows some minor deactivation. However, this decay is certainly far away from the current decrease on the PB-decorated electrode, in agreement with the good FTO chemical stability reported under different pH and potential conditions, compared with other TCOs like indium tin oxide (ITO) or antimony-doped tin oxide (ATO).[44–45] Therefore, the current decay of the AAO/FTOCoHCF sample during the first hours is assigned to the mechanical loss of poorly attached CoHCF crystallites, which becomes less relevant as the experiment proceeds. The current density reaches c.a. 50 % and 20 % of its initial value after c.a. 4 and 50 hours, respectively. However, this phenomenon presumably takes place only at the very first use of the electrode and does not lead to the full depletion of the active sites as it was confirmed by the post-reaction characterization shown above. AAO/FTO/PB shows to be stable with a decay of the current density of 0.17 mA cm^{-2} for the last 40 hours. A steady-state current density of 1.85 mA cm^{-2} is obtained after 100 hours polarization at 2.2 V vs, RHE without any further significant sign of deterioration. This denotes the long-term robustness of the proposed electrode, which is not comparable with the robustness reported in most water oxidation studies in half-cell configuration, typically evaluated for less than 24 h. One can find in Supplementary information a video (Video S1) where oxygen bubbles evolving from the electrode surface during the CA at 2.2 V vs. RHE can be observed.

The stability of the AAO/FTO/PB electrode has also been confirmed at 2.4 V vs. RHE by using a new AAO/FTO/PB electrode prepared in a similar way than the previous one. A stable current density of 2.6 mA cm^{-2} is obtained at this voltage after 100 hours (See Figure S2 in Supplementary Information). A faradaic efficiency towards oxygen evolution reaction closed to 100 % has been confirmed by in-situ measuring, during the latter CA, the increase of oxygen concentration in the anode gas headspace using a FOXY probe. The similarity between the O_2 production experimentally measured during a given polarization time and the theoretical (faradaic) O_2 production calculated from the electric charge transferred during the same period can be clearly observed in Figure S3 in Supplementary Information.

In order to prove the superior properties of the AAO/FTO/PB electrode with respect to an analogous catalyst prepared on a flat surface support, i. e. instead of AAO, additional electrodes have been prepared by FTO deposition on glass substrates and subsequent Prussian blue catalyst deposition by following a similar procedure than that carried out on AAO supports. ESEM images of both glass- and AAO-supported FTO layers are observed in Figure S4. A smoother FTO surface is apparently obtained on flat glass compared to the FTO layer grown on AAO where a higher roughness can be appreciated because of a greater presence of defects on the latter substrate. Figure S5 shows the EDX and XRD characterization of the Glass/FTO/PB electrode and the corresponding blank electrode (i. e., in absence of PB). A much lower presence of CoHCF on the Glass/FTO surface can be deduced with respect to the EDX spectra and XRD diffractograms obtained with the AAO-supported electrode (i. e., Figure 6), which can be attributed to a stronger attachment of the catalyst nanoparticles on the rough surface of the latter electrode. The same electrochemical tests than those shown in Figures 8–10 have been performed on both Glass/FTO/PB and Glass/FTO (See Figures S6–8 in Supplementary information). From the linear sweep voltammetry measurement (Figure S6) much lower current density values can be observed in the same voltage scan than those values previously shown in Figure 8 with AAO-supported catalyst, as expected due to the lower roughness of the FTO layer deposited on the glass support. Higher Tafel slope is also obtained with Glass/FTO/PB (Figure S7) than with AAO/FTO/PB (Figure 9). Finally, in the chronoamperometry performed at 2.2 V vs. RHE for 100 h with the glass-supported electrode (Figure S8), a continuous decrease of the current density has been observed during the whole polarization, reaching a final current density of i. e., 0.78 mA cm^{-2}, in contrast to the stable current density obtained with the AAO-supported electrode, i. e., 1.85 mA cm^{-2} (Figure 10). Thus, the use of anodic aluminum oxide as catalyst support is confirmed to provide not only higher electrocatalytic activity but also higher electrode stability. We attribute this effect to the higher FTO layer roughness obtained on AAO substrate and the stronger attachment of the PB nanoparticles on this surface.

If we consider the electrocatalytic performances reported in benchmarking studies of water oxidation catalysts,[46–47] in terms of overpotential required to obtained a given current density after 2 or 24 hours, it is clear that the results obtained with the studied AAO/FTO/PB electrode at pH 7 are still not comparable with those obtained with either Ru and Ir catalysts at pH 0 or electrodes based on Co, Ni and Fe, among others, at pH 14. However, from the obtained results it can be stated that the electrocatalytic activity of the AAO/FTO/PB catalyst for water oxidation is higher than that previously reported with FTO/PB electrodes[28–29] and other earth-abundant materials-based electrodes.[48–49] Thus, the feasibility of FTO-covered AAO as a conductive and efficient catalyst support for electrocatalytic processes is demonstrated herein and, particularly, for water electrolysis at neutral pH and ambient conditions. It should also be noted that the proposed configuration is prone to further optimization, by tuning the porous structure of the AAO and by improving the deposition method for both the FTO crystallites and the catalyst nanoparticles.

3. Conclusions

An efficient and simple route to achieve a significant electrical conductivity on an alumina surface (AAO) was established by FTO deposition via spray pyrolysis. From the results of X-ray diffraction, I–V curve and ESEM images we conclude that the as-deposited FTO crystallite size increases with deposition time, while the film electrical resistivity decreases down to a basal minimum. We decorated an optimized FTO/AAO composite with Prussian blue (PB)-type cobalt hexacyano-ferrate nano-

particles, a promising earth-abundant metal-based electrocatalyst for water oxidation, exhibiting excellent performance in terms of electrochemical activity and stability during the oxygen evolution reaction. Our results open interesting possibilities for the development of electrode supports from intrinsic insulators, possessing very high surface areas, such as AAO. Taking advantage of the latter, surface modification with a conducting layer allows their transformation into functional electrodes. In neutral media, our AAO/FTO/PB composite electrodes promote electrochemical water splitting at higher current densities that any other non-noble metal-based electrodes, with long term stability (> 100 h). In this proof of concept, we also observed a synergic relation between the porous alumina and the conducting phase, with enhanced FTO conductivity due to the presence of induced defects in conducting component.

Experimental Section

Synthesis of the Electrodes

Fluorine-doped tin oxide was deposited on AAO substrates. The precursor solution was synthesized from Sn(IV) salts, using $SnCl_4 \cdot 5H_2O$. A 0.23 M solution was prepared in a mixture of polar solvents: CH_3CH_2OH 99.9 % and deionized H_2O in a ratio of 9 : 1, respectively. 0.27 g of NH_4F were used as the dopant source, to obtain a concentration of 5 wt.% of F with respect to the amount of Sn present in the stock solution, i. e. resulting in a F/Sn = 0.05 ratio. Subsequently the ethanolic solution was heated at 80 °C for 60 min to hydrolyze the Sn^{+4} ion and, in this way, obtain the $Sn(OH_x)$ solution. This precursor solution was deposited onto AAO membranes using a home-made spray pyrolysis system. The configuration scheme of a similar system has been previously reported.[50] AAO substrates with pores around 220 nm of diameter and 60 μm of thickness (Sigma-Aldrich) were used. The deposition temperature, controlled within ± 1°C, was set at 440 °C and the deposition times were in the range from 10 to 120 min including deposition on both sides of the AAO substrate (i. e. from 5 to 60 min on each side). FTO was also deposited on glass substrates at the same deposition times. The latter samples were used to obtain the FTO deposition rate by estimating the optical thickness in each case from the transmittance spectrum, as reported elsewhere.[35] FTO on glass was also deposited as reference support for the water oxidation catalyst, in order to compare the electrocatalytic performance of AAO-supported electrodes and those supported on a flat surface.

Prussian blue catalyst was obtained via the dip coating technique. Two solutions were prepared for the depositions. Solution A: 0.01 M $K_3[Fe(CN)_6]$, and solution B: 0.01 M $Co(NO_3)_2 \cdot 6H_2O$. Five deposition cycles were performed, where AAO/FTO and Glass/FTO samples were dipped, first, in solution A and, second, in solution B for 15 minutes in each case, followed by air drying overnight. The deposition process was carried out under magnetic stirring and only an area of 1 cm^2 from each electrode was dipped. All chemicals used in this study were of analytical grade and provided by Sigma-Aldrich.

Characterization of the Electrodes

XRD patterns were obtained from the different samples by using a Siemens EM-10110BU model D5000 diffractometer, operating with the Cu Kα line (λ = 1.541 Å). ESEM images and EDX spectra were acquired in a QUANTA600 equipment from FI company under high vacuum conditions. The electron microscope was operated at 20 kV. This physicochemical characterization was carried out both before and after the electrocatalytic tests. I–V measurements were performed in a coplanar configuration using a Keithley 2400 digital picoammeter/voltage source from Keithley Instruments, Inc.. The voltage was applied between the silver epoxy contacts spaced 1 cm on each surface and the current was collected using the same equipment. So, to obtain the sheet (in-plane) electrical resistance of the different FTO layers between these points, the slope of the resultant I–V curve was used to obtain the surface resistance value corresponding to each coating condition. Then the respective resistivities were estimated by considering the FTO optical thicknesses, as was also accomplished in previous works.[35]

Electrocatalytic Tests

The electrochemical experiments were performed at room temperature and atmospheric pressure in half-cell configuration (See Figure S9 in Supplementary Information) by using a Biologic SP-150 potentiostat and a buffer electrolyte prepared in 50 mM KPi (pH 7) containing 1 M KNO_3. A H-cell was used where the anode and cathode compartments were separated by a porous glass frit and all the experiments were carried out under magnetic stirring at c.a. 1000 rpm in order to remove the O_2 and H_2 bubbles from the electrodes (see Video S1 in Supplementary Information). Linear Sweep Voltammetry (LSV) and Chronoamperometry (CA) measurements were performed by employing Ag/AgCl (3.5 M KCl) from ALS as reference electrode, Pt mesh as counter electrode (cathode) and AAO/FTO/PB or Glass/FTO/PB as working electrode (anode). Blank measurements were also carried out with AAO/FTO and Glass/FTO samples. Before the electrochemical measurements the electrical contacts were made by tin welding and silver conductive epoxi from RS COMPONENTS LTD. on the Glass- and AAO-supported electrodes, respectively, in electrode areas not covered by Prussian blue. In all cases the electrical contacts were finally coated by epoxy adhesive from RS COMPONENTS LTD and were avoided to dip into the electrolyte during the electrocatalytic tests.

All potentials measured in this work were iR corrected by the current interruption technique and converted to the reversible hydrogen electrode (RHE) scale through equation 1.

$$E_{(RHE)} = E_{(Ag/AgCl)} + 0.059\ pH + E^0_{(Ag/AgCl)} \quad (1)$$

Where $E_{(Ag/AgCl)}$ is the measured working potential and $E^0_{(Ag/AgCl)}$ is 0.205 V at 25 °C. Then overpotential (η) was calculated from equation 2.

$$\eta = E_{(RHE)} - E^0_{cell} \quad (2)$$

Where E^0_{cell} is the standard potential of the water electrolysis cell which is 1.229 V at 25 °C. All current density values have been normalized per electrode geometrical area. The experimental procedure carried out for the in-situ oxygen evolution measurement is described in Supplementary information.

Acknowledgements

We would like to acknowledge financial support from the Spanish Ministerio de Economía y Competitividad (MINECO) through project CTQ2015-71287-R and the Severo Ochoa Excellence Accred-

itation 2014-2018 SEV-2013-0319; and the Generalitat de Catalunya (2017-SGR-1406 and the CERCA Programme). FAGP thanks the Marie Curie COFUND Action from the European Commission for co-financing his postdoctoral fellowship.

Conflict of Interest

The authors declare no conflict of interest.

Keywords: anodic aluminium oxide · fluorine-doped tin oxide · Prussian Blue · water electrolysis · water electrooxidation

[1] W. Lee, S. J. Park, *Chem. Rev.* 2014, *114*, 7487–7556.
[2] A. M. Md Jani, D. Losic, N. H. Voelcker, *Prog. Mater. Sci.* 2013, *58*, 636–704.
[3] Z. A. Hamid, M. T. A. El-Khair, M. H. Gomaa, F. A. Morsy, N. A. A. Khalifa, *Int. J. Nanopart.* 2014, *7*, 231–250.
[4] H. Zhao, M. Zhou, L. Wen, Y. Lei, *Nano Energy* 2015, *13*, 790–813.
[5] H. Dang, V. P. Singh, S. Guduru, S. Rajaputra, Z. D. Chen, *Nano Res.* 2015, *8*, 3186–3196.
[6] H. Zhang, J. H. Kim, J. S. Lee, *Adv. Funct. Mater.* 2017, *27,* 1702428.
[7] A. Brzózka, A. Jeleń, A. M. Brudzisz, M. M. Marzec, G. D. Sulka, *Electrochim. Acta* 2017, *225*, 574–583.
[8] H. E. Cheng, S. Y. Lin, D. C. Tian, *J. Electrochem. Soc.* 2014, *161*, E202–E206.
[9] S. Garbarino, A. Ponrouch, E. Bertin, D. Guay, *Mater. Res. Soc. Symp. Proc.* 2011, *1311*, 7–12.
[10] W. Yan, D. Wang, G. G. Botte, *J. Appl. Electrochem.* 2015, *45*, 1217–1222.
[11] T. Y. Shin, S. H. Yoo, S. Park, *Chem. Mater.* 2008, *20*, 5682–5686.
[12] H. Wang, C. Xu, F. Cheng, M. Zhang, S. Wang, S. P. Jiang, *Electrochem. Commun.* 2008, *10*, 1575–1578.
[13] J. Cui, Y. Wu, Y. Wang, H. Zheng, G. Xu, X. Zhang, *J. Nanosci. Nanotechnol.* 2013, *13*, 1149–1152.
[14] S. Altuntas, F. Buyukserin, *Appl. Surf. Sci.* 2014, *318*, 290–296.
[15] E. Wierzbicka, G. D. Sulka, *Sens. Actuators B* 2016, *222*, 270–279.
[16] M. Schalenbach, A. R. Zeradjanin, O. Kasian, S. Cherevko, K. J. J. Mayrhofer, *Int. J. Electrochem. Sci.* 2018, *13*, 1173–1226.
[17] S. Y. Tee, K. Y. Win, W. S. Teo, L. D. Koh, S. Liu, C. P. Teng, M. Y. Han, *Adv. Sci.* 2017, *4*, 1600337.
[18] J. Qi, W. Zhang, R. Cao, *ChemCatChem* 2018, *10*, 1206–1220.
[19] S. Park, Y. Shao, J. Liu, Y. Wang, *Energy Environ. Sci.* 2012, *5*, 9331–9344.
[20] E. Özer, C. Spöri, T. Reier, P. Strasser, *ChemCatChem* 2017, *9*, 597–603.
[21] X. Liang, R. Dong, D. Li, X. Bu, F. Li, L. Shu, R. Wei, J. C. Ho, *ChemCatChem* 2018, *10*, 4555–4561.
[22] Y. Yi, G. Weinberg, M. Prenzel, M. Greiner, S. Heumann, S. Becker, R. Schlögl, *Catal. Today* 2017, *295*, 32–40.
[23] S. Schlicht, S. Haschke, V. Mikhailovskii, A. Manshina, J. Bachmann, *ChemElectroChem* 2018, *5*, 1259–1264.
[24] N. Linck, A. Peek, B. J. Hinds, *ACS Appl. Mater. Interfaces* 2017, *9*, 30964–30968.
[25] J. R. Galán-Mascarós, *ChemElectroChem* 2014, *2*, 37–50.
[26] M. I. Jamesh, X. Sun, *J. Power Sources* 2018, *400*, 31–68.
[27] M. Aksoy, S. V. K. Nune, F. Karadas, *Inorg. Chem.* 2016, *55*, 4301–4307.
[28] E. P. Alsaç, E. Ülker, S. V. K. Nune, Y. Dede, F. Karadas, *Chem. Eur. J.* 2018, *24*, 4856–4863.
[29] S. Pintado, S. Goberna-Ferrón, E. C. Escudero-Adán, J. R. Galán-Mascarós, *J. Am. Chem. Soc.* 2013, *135*, 13270–13273.
[30] F. S. Hegner, I. Herraiz-Cardona, D. Cardenas-Morcoso, N. López, J. R. Galán-Mascarós, S. Gimenez, *ACS Appl. Mater. Interfaces* 2017, *9*, 37671–37681.
[31] B. Rodríguez-García, Á. Reyes-Carmona, I. Jiménez-Morales, M. Blasco-Ahicart, S. Cavaliere, M. Dupont, D. Jones, J. Rozière, J. R. Galán-Mascarós, F. Jaouen, *Sustainable Energy Fuels* 2018, *2*, 589–597.
[32] L. Han, P. Tang, Á. Reyes-Carmona, B. Rodríguez-García, M. Torréns, J. R. Morante, J. Arbiol, J. R. Galan-Mascaros, *J. Am. Chem. Soc.* 2016, *138*, 16037–16045.
[33] D. Mohanta, M. Ahmaruzzaman, *RSC Adv.* 2016, *6*, 110996–111015.
[34] R. A. Afre, N. Sharma, M. Sharon, *Rev. Adv. Mater. Sci.* 2018, *53*, 79–89.
[35] F. A. Garcés, N. Budini, R. R. Koropecki, R. D. Arce, *Thin Solid Films* 2013, *531*, 172–178.
[36] E. Ching-Prado, A. Watson, H. Miranda, *J. Mater. Sci. Mater. Electron.* 2018, *29*, 15299–15306.
[37] K. H. Kim, B. R. Koo, H. J. Ahn, *Ceram. Int.* 2018, *44*, 9408–9413.
[38] Y. Gao, Y. Lin, J. Chen, Q. Lin, Y. Wu, W. Su, W. Wang, Z. Fan, *Nanoscale* 2016, *8*, 13280–13287.
[39] A. E. Hassanien, H. M. Hashem, G. Kamel, S. Soltan, A. M. Moustafa, M. Hammam, A. A. Ramadan, *Int. J. Thin Film. Sci. Tec.* 2016, *5*, 55–65.
[40] H. M. Yates, P. Evans, D. W. Sheel, Z. Remeš, M. Vanecek, Ü. Dagkaldiran, A. Gordijn, F. Finger, *Int. J. Nanotechnol.* 2009, *6*, 816–827.
[41] A. Bleuzen, C. Lomenech, V. Escax, F. Villain, F. Varret, C. Cartier Dit Moulin, M. Verdaguer, *J. Am. Chem. Soc.* 2000, *122*, 6648–6652.
[42] M. Afzaal, H. M. Yates, A. Walter, S. Nicolay, C. Ballif, *J. Mater. Sci.* 2017, *5*, 4946–4950.
[43] F. Z. Dahou, L. Cattin, J. Garnier, J. Ouerfelli, M. Morsli, G. Louarn, A. Bouteville, A. Khellil, J. C. Bernède, *Thin Solid Films* 2010, *518*, 6117–6122.
[44] J. D. Benck, B. A. Pinaud, Y. Gorlin, T. F. Jaramillo, *PLoS One* 2014, *9*, e107942.
[45] S. Geiger, O. Kasian, A. M. Mingers, K. J. J. Mayrhofer, S. Cherevko, *Sci. Rep.* 2017, *7*, 4595.
[46] C. C. L. McCrory, S. Jung, J. C. Peters, T. F. Jaramillo, *J. Am. Chem. Soc.* 2013, *135*, 16977–16987.
[47] C. C. L. McCrory, S. Jung, I. M. Ferrer, S. M. Chatman, J. C. Peters, T. F. Jaramillo, *J. Am. Chem. Soc.* 2015, *137*, 4347–4357.
[48] M. Martin-Sabi, J. Soriano-López, R. S. Winter, J. J. Chen, L. Vilà-Nadal, D. L. Long, J. R. Galán-Mascarós, L. Cronin, *Nat. Catal.* 2018, *1*, 208–213.
[49] S. Haschke, Y. Wu, M. Bashouti, S. Christiansen, J. Bachmann, *ChemCatChem* 2015, *7*, 2455–2459.
[50] B. Gottlieb, R. Koropecki, R. Arce, R. Crisalle, J. Ferron, *Thin Solid Films* 1991, *199*, 13–21.